Cubic defects: comparing the eight-state system with its two-level approximation

Cubic defects: comparing the eight-state system with its two-level approximation

Peter Nalbach and Orestis Terzidis

Institut für Theoretische Physik, Philosophenweg 19, 69120 Heidelberg, Germany

Abstract. Substitutional defects in a cubic symmetry (such as a lithium defect in a KCl host crystal) can be modelled appropriately by an eight-state system. Usually this tunnelling degree of freedom is approximated by a two-level system. We investigate the observable differences between the two models in three contexts. First, we show that the two models predict different relations between the temperature dependence of the specific heat and that of the static susceptibility. Second, we demonstrate that in the presence of external forces (pressure and electric field) the eight-state system shows features that cannot be understood within the framework of the two-level approximation. In this context we propose an experiment for measuring the parameter governing tunnelling along the face diagonal. Finally, we discuss the differences between the models appearing for strongly coupled pairs. Geometric selection rules and particular forms of asymmetry lead to clear differences between the two models.

1. Introduction

Quantum tunnelling of substitutional defect ions in alkali halide crystals leads to particular low-temperature properties [1]. Due to their misfit in size or shape, such defect ions are confined to a potential energy landscape with a few degenerate potential wells. At low temperatures, thermally activated crossing over the barriers is inhibited, and the defect ion passes through the barrier by quantum tunnelling; typically, at a few kelvin, hopping becomes relevant. The potential energy landscape in which the defect ion moves is produced by the host crystal, and therefore reflects its symmetry, which for most alkali halide crystals is cubic (e.g. the fcc structure of potassium chloride). There are only three multi-well potentials which are consistent with this symmetry: twelve wells at the edges of a cube, six wells at the centres of the surfaces, and eight wells at the corners of a cube. In all cases the edges of the cube lie along the crystal axes, and the multi-well structure leads to off-centre sites for the defect ion. The off-centre position has two immediate consequences: it separates the centres of charge, and leads to a local distortion of the crystal. Hence both an electric dipole moment and an elastic quadrupole moment are connected to the defect, which can thus interact with lattice vibrations, external fields, or neighbouring defects. Consequently, only at low defect concentrations can one describe the situation in terms of isolated tunnelling systems. With rising concentration, pairs, triples, etc, of defects become involved, until finally one faces a complicated many-body system [4, 10].

A standard example of tunnelling defects is that of potassium chloride doped with a small proportion of lithium ions (KCl:Li). This system is well described in terms of isolated defects for concentrations up to say 20 ppm. The minima of the system lie at the corners of a cube ($d \approx 1.4$ Å); in the low-temperature regime the relevant degree of freedom is thus an

eight-state system (ESS). There are three different matrix elements for tunnelling: (i) along the edges of the cube, k; (ii) along a face diagonal, f; and (iii) along a space diagonal, r; edge tunnelling dominates the defect spectrum [5] for simple geometric reasons: the edge is the shortest distance between the potential minima. Neglecting face and space diagonal tunnelling, the problem factorizes into three two-level systems (TLS); this much simpler model is often used for the description of the defect.

In this paper we want to study to what extent the TLS is a good approximation for the ESS (and hence to what extent tunnelling along the face and space diagonal on the one hand and the particular geometry of the defect on the other are negligible). We find that in most contexts the TLS approximation is in fact acceptable; still there are several experimentally observable features which cannot be explained within the TLS approximation.

The plan of the paper is as follows. In section 2 a tensorial Hamiltonian for the eight-state system is introduced. Physical properties such as the specific heat and the static dielectric susceptibility are derived and compared with the results from using the two-level approximation. In section 3 we discuss the coupling of the eight-state system to static external electric or strain fields. We propose an experiment for measuring directly the parameter governing tunnelling along a face diagonal. (This parameter will dominate all of the corrections to the TLS results.) In section 4 strongly coupled pairs of eight-state systems are considered. We discuss the situation by means of group theory, and investigate in particular the relevance of different asymmetry terms for echo experiments. Finally section 5 gives a conclusion.

2. Specific heat and static susceptibility

2.1. Theory

Before going into a discussion of the ESS we would like to summarize some of the well-known features of a TLS. This system describes a particle in a double-well potential depending on one single coordinate (instead of the three space dimensions of the ESS). The tunnelling Hamiltonian of the TLS reads in the 'local' basis (i.e. the basis where σ_z represents the position to the 'left' or 'right' of the particle)

$$H = k_0 \sigma_x. \tag{1}$$

The symbols σ_x, σ_z denote the Pauli matrices. The only parameter entering the system is the tunnelling parameter k_0 describing tunnelling between the left-hand state and the right-hand state. It is given by the WKB formula

$$k_0 = -E_0 \exp\left\{-\frac{d}{2\hbar}\sqrt{2mV_0}\right\} < 0. \tag{2}$$

Here the energy E_0 is the oscillator frequency of a well, d is the distance between the two wells, m is the mass of the tunnelling particle, and V_0 is the barrier height. Since σ_z represents the position operator, all external fields couple to the product $F\sigma_z$, where F stands for the amplitude of an external field (such as a static electric or strain field and an electromagnetic or acoustic wave).

Two characteristic features of the TLS have been studied in numerous experiments: the temperature dependence of the specific heat (the Schottky anomaly)

$$c_v(T) = \frac{k_0^2}{k_B T^2} \operatorname{sech}^2(\beta k_0) \tag{3}$$

and the temperature dependence of the static susceptibility

$$\chi_{stat}(T) = \frac{p^2}{\hbar\epsilon_0}\frac{1}{k_0}\tanh(\beta k_0). \tag{4}$$

Let us now ask what observable differences appear if we consider the ESS. In order to find an answer, we derive the corresponding formulae of this system and compare them to those of the TLS. For the ESS, three coordinates determine the wave function in the local basis $\{|xyz\rangle\}$ with $x, y, z = \pm 1$; the origin of the system is located at the centre of the cube, and the axes point along its edges. The position operator now becomes a vector:

$$\hat{r} = \frac{d}{2}\begin{pmatrix} r_x \\ r_y \\ r_z \end{pmatrix} = \frac{d}{2}\begin{pmatrix} \sigma_z \otimes 1 \otimes 1 \\ 1 \otimes \sigma_z \otimes 1 \\ 1 \otimes 1 \otimes \sigma_z \end{pmatrix} \tag{5}$$

where the symbol $\otimes$ denotes a tensor product and each factor stands for one coordinate. The tunnelling Hamiltonian of the ESS can be decomposed into tensor products; edge tunnelling along the x-direction for example is described by $k(\sigma_x \otimes 1 \otimes 1)$. Tunnelling along the face or space diagonal involves more than one coordinate; the corresponding Hamiltonian is given by

$$\hat{H}_0 = k(1 \otimes 1 \otimes \sigma_x + 1 \otimes \sigma_x \otimes 1 + \sigma_x \otimes 1 \otimes 1)$$
$$+ f(1 \otimes \sigma_x \otimes \sigma_x + \sigma_x \otimes 1 \otimes \sigma_x + \sigma_x \otimes \sigma_x \otimes 1) + r(\sigma_x \otimes \sigma_x \otimes \sigma_x). \tag{6}$$

Here k, f, and r are the amplitudes for tunnelling along an edge, a face diagonal, and a space diagonal. Let us next write down the elastic and electric momenta connected with the defect. The separation of charge which arises from the off-centre position causes an electric dipole moment

$$\boldsymbol{p} = q\boldsymbol{r} \qquad p = \frac{\sqrt{3}}{2}qd. \tag{7}$$

The corresponding energy of interaction with an external electric field $\boldsymbol{F}$ reads

$$W_F = -\sum_i F_i p_i. \tag{8}$$

Moreover the defect distorts the host crystal locally, producing thus an elastic moment. Würger [4] derived as the leading contribution a quadrupole moment:

$$Q_{ij} = \frac{4}{d^2}r_i r_j(1 - \delta_{ij}). \tag{9}$$

Remember here that r_i is a component of the position operator. The corresponding energy of interaction with a strain field is given by

$$W_\epsilon = -g\sum_{i,j} Q_{ij}\varepsilon_{ij} \tag{10}$$

where g is a coupling constant and ε_{ij} is the tensor of the distortion produced by the strain field. In the static case this tensor can be derived from the exerted pressure using standard elastomechanical relations [3]; in the case of acoustic waves it reads $\varepsilon_{ij} = (1/2)(\partial_j u_i + \partial_i u_j)$, where $\boldsymbol{u}$ denotes the amplitude of the phonon.

Just like for the TLS, the tunnelling parameters can be found with the WKB formula (2). Assuming that the heights of all of the potential barriers are of the same order of magnitude, the three tunnelling parameters differ only for a simple geometric reason: the distance separating the minima is different (the edge of a cube is shorter than a face diagonal, etc). One concludes that $|k| > |f| > |r|$. Hence in a first approach one can neglect f and

r. Then the Hamiltonian (6) factorizes, and three independent TLS remain, one for each spatial direction. This is just the two-level approximation, keeping in mind the factor of three: one ESS (with $f = r = 0$) is equivalent to three TLS. One can then conclude that as soon as f and r become non-negligible, differences between the ESS and the TLS will arise.

Let us go further in our analysis of the ESS. The simple structure of the problem allows the exact calculation of its spectrum and eigenvectors. They are given by the following scheme:

$$
\begin{aligned}
E_3 &= -3k + 3f - r: & |---\rangle \\
E_2 &= -k - f + r: & |+--\rangle, |-+-\rangle, |--+\rangle \\
E_1 &= k - f - r: & |++-\rangle, |+-+\rangle, |-++\rangle \\
E_0 &= 3k + 3f + r: & |+++\rangle
\end{aligned}
\tag{11}
$$

with

$$
|\pi_x \pi_y \pi_z\rangle = \frac{1}{\sqrt{8}} \sum_{x,y,z=\pm 1} f_x^{\pi_x} f_y^{\pi_y} f_z^{\pi_z} |xyz\rangle
\tag{12}
$$

$$
f_j^{\pi_j} = \exp\left(\frac{i\pi}{4}(1 - \pi_j)(1 - j)\right).
\tag{13}
$$

Here $\pi_i = \pm$ denotes the parity of the wave function in the i-direction. The spectrum consists of four levels with a threefold degeneracy of the second and the third level. The transitions shown in figures 1(a) and 1(b) are derived from the electric and acoustic interactions given above. As an explicit example we consider an electric field oscillating in the y-direction. Figure 1(a) gives a complete scheme for the possible transitions.
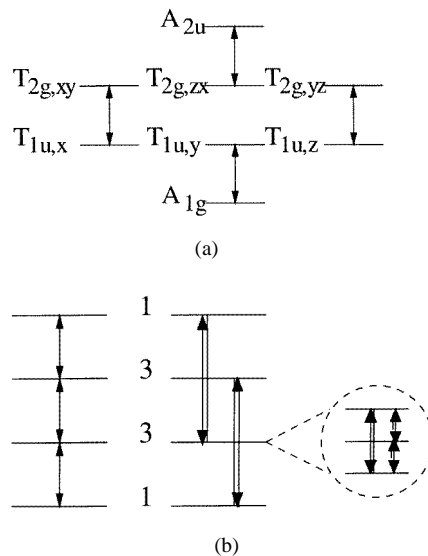

(a)

(b)

Figure 1. (a) Selection rules of the ESS for an electric field oscillating in the [100] direction, together with the Schoenflies notation. (b) Possible electric (single arrows) and acoustic (double arrows) selection rules for the ESS.

Every geometric constellation has its specific selection rules; we refrain from giving a complete list of all of these possibilities, and instead propose in figure 1(b) a schematic

diagram where all possible transitions are shown. Note that for the electric transition, one of the parities π_i changes its sign, whereas for the acoustic transitions, two parities change their signs. Hence in the acoustic case, the product $\pi_1\pi_2\pi_3$ is conserved.

There are three electric transitions with almost the same frequency, $\sim 2k$. In the acoustic case, there are two transitions with frequency $\sim 4k$, and two 'inside' the degenerate triplets. (These transitions are visible as soon as some perturbation destroys the degeneracy; cf. section 3.) The fact that for both couplings only one transition frequency appears is crucial for the validity of the two-level approximation: by construction the TLS would not be able to reflect more than one single energy. Indeed the approximation cannot account for the fact that the frequency induced by electric fields differs from that induced by acoustic fields.

Let us now turn to the temperature dependence of the specific heat and that of the static susceptibility. The partition function is given by

$$Z = \text{Tr}(e^{-\beta H}) = \sum_l \eta_l e^{-\beta \mathcal{E}_l} \qquad \beta = \frac{1}{k_B T}$$

where η_l denotes the degree of degeneracy of the eigenvalue $\mathcal{E}_l$, and k_B is the Boltzmann constant. The free energy of the system is then given by $F = -k_B T \ln Z$, and the specific heat reads

$$c_v(T) = \frac{k_B \beta^2}{Z^2} \sum_{i<j} \eta_i \eta_j (\mathcal{E}_i - \mathcal{E}_j)^2 e^{-\beta(\mathcal{E}_i + \mathcal{E}_j)}. \tag{14}$$

Inserting the energies given in (11), one finds for the specific heat of the ESS

$$c_v(T) = \frac{k_B \beta^2}{Z^2}\{(6k + 2r)^2 e^{-6\beta f} + 3(4k - 4f)^2 e^{-\beta(-2k+2f-2r)}$$
$$+ 9(2k - 2r)^2 e^{2\beta f} + 3(2k - 4f + 2r)^2 e^{-\beta(-4k+2f)}$$
$$+ 3(2k + 4f + 2r)^2 e^{-\beta(4k+2f)} + 3(4k + 4f)^2 e^{-\beta(2k+2f+2r)}\}. \tag{15}$$

This expression reduces to the corresponding formula for the TLS when one sets $f = r = 0$.

Let us now write down the susceptibility χ. The response of the ESS to an external field is given by the commutator formula [7]

$$\chi_{ij} = \frac{i}{\hbar}\langle[p_i(t), p_j(t_0)]\rangle \Theta(t - t_0)$$

with the time-dependent dipole operator $p(t) = \exp(i/\hbar \hat{H} t)\hat{p} \exp(-i/\hbar \hat{H} t)$, and the Gibbs mean value $\langle \cdot \rangle = \text{Tr}(\cdot \exp(-\beta \hat{H}))/Z$. In order to find the static susceptibility, one has to look at the real part of the Laplace transform for zero frequency. This leads to

$$\chi_{x,x}^{stat}(T) = \frac{2}{Z}\frac{p^2}{\hbar\epsilon_0}\left\{[e^{\beta(3k+3f+r)} - e^{-\beta(k-f-r)}]\frac{1}{(2k+4f+2r)}\right.$$
$$+ 2[e^{\beta(k+f-r)} - e^{-\beta(-k-f+r)}]\frac{1}{(2k-2r)}$$
$$\left. + [e^{-\beta(-k-f+r)} - e^{\beta(-3k+3f-r)}]\frac{1}{(2k-4f+2r)}\right\}. \tag{16}$$

All other elements of the susceptibility tensor are then known: the symmetry of the problem implies $\chi_{x,x} = \chi_{y,y} = \chi_{z,z}$ and $\chi_{x,y} = \chi_{x,z} = \chi_{y,z} = 0$. Again this result reduces to the corresponding formula for the TLS in the case of vanishing face and space diagonal parameters.

At first sight, almost no contrast between the two models emerges from the above formulae. Taking reasonable values for f and r (say $r/f = f/k \approx$ 10–20%), the plots look practically the same. The question arises of whether there is at all a simple observable feature which distinguishes between the TLS and the ESS. Such a criterion does indeed exists. It is based on the observation that for the TLS the relation $k_0^2 \, \partial_T \chi = c_V$ holds, whereas this is not true for the ESS. One simple consequence is that the turning point of the susceptibility and the maximum of the specific heat *coincide* for a TLS, whereas they occur at *different* temperatures for the ESS. To be more explicit: defining

$$
\begin{aligned}
T_{\text{max}}: \quad & \frac{\partial}{\partial T} c_V (T = T_{\text{max}}) = 0 \\
T_{\text{turn}}: \quad & \frac{\partial^2}{\partial T^2} c_V (T = T_{\text{turn}}) = 0
\end{aligned}
\tag{17}
$$

one finds that for the TLS

$$
T_{\text{max}} = T_{\text{turn}}
$$

whereas for the ESS

$$
T_{\text{max}} < T_{\text{turn}}
\tag{18}
$$

holds. It is not possible to give an explicit expression for $\Delta T = T_{\text{turn}} - T_{\text{max}}$ as a function of f and k, since transcendental equations are involved. Instead we plot in figure 2 ΔT as a function of f with the parameter k. It turns out that ΔT depends only very weakly on k for 0.5 K $< |k|/k_B <$ 1.5 K, and that a linear relation $\Delta T \approx 0.85|f|/k_B$ holds approximately.
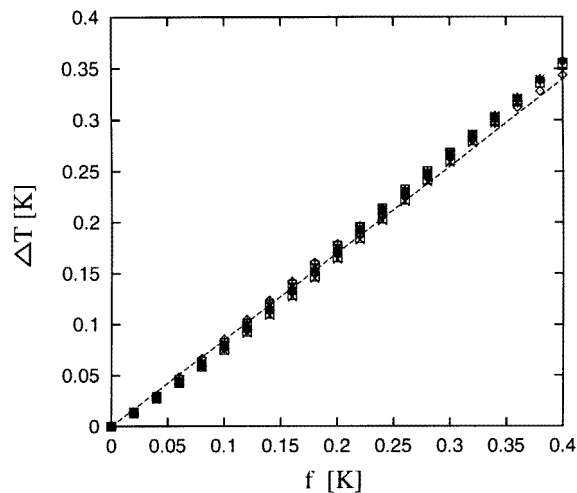

Figure 2. $\Delta T = T_{\text{turn}} - T_{\text{max}}$ as a function of $|f|$. The different points indicate different values of $|k|$ between 0.5 and 1.5 K. The line is a linear fit with a slope of 0.85.

As the ESS is the more realistic model, the deviation $T_{\text{max}} \neq T_{\text{turn}}$ should be visible in experiments. This will be discussed in the following.

Note that Fiory [8] has shown that even for low concentrations the 'Schottky anomaly' of the specific heat gets distorted by the dipole–dipole interaction between the defects, and a similar effect is expected for the dielectric susceptibility. Both effects—the interaction and the face tunnelling—might interfere in a real sample. But by examining probes with

different defect concentrations, it is in principle possible to distinguish between the two effects; any change depending on a variation of concentration results from interactions, while effects that are independent of such a variation arise due to face diagonal tunnelling.

2.2. Experimental data

Let us now take a look at the experimental data. We will make use of the specific heat data from Pohl and co-workers [2] and the dielectric susceptibility data from Enss *et al* [6]. Since f will be the leading correction to the TLS approximation, we will neglect r in the following. We then have two fitting parameters, f and k, and we can look for the optimal set in order to reproduce the data. But in fact there is a third undetermined quantity: the defect concentration of the probe cannot be fixed accurately. But the concentration varies only over a very small range, so we focus on the tunnelling parameters. All parameter sets consistent with the experimental data (obtained by fitting the relations (15) and (16) to the data) do in fact confirm the relation $T_{\max} < T_{\text{turn}}$.

For a further comparison of the two models, we will proceed as follows. The TLS is completely specified by the parameter k_0, whereas the ESS is specified by the pair (k, f). Now one can ask what relation between the ESS parameter pair (k, f) and the single TLS parameter k_0 must hold in order to produce either the same maximum of c_v or the same turning point of χ. The c_V-maxima of the two models coincide if the equation $k + 1.7f \approx k_0$ is fulfilled (which can be verified by differentiating and solving a transcendental equation). The turning points of χ are the same if $k + 2.7f \approx k_0$ holds. This shows that a TLS analysis does indeed yield different tunnelling parameters for the two experiments, which is counterintuitive; after all, the same degree of freedom produces both anomalies. Usually such effects were thought to be due to experimental uncertainty; but the above considerations show that the difference is a systematic consequence of tunnelling along the face diagonal. On the basis of the difference between $T_{\max}$ and T_{turn}, one can estimate an optimal parameter set. In order to do so, one has to solve a set of transcendental equations, where $T_{\max}$ and T_{turn} are given by the data, and f and k are the unknown variables. We have given the result in table 1.

Table 1. The parameter set consistent with experimental data. In the lower part of the table, effective values for a TLS are listed.

	^{6}Li	^{7}Li
k/k_B	−0.63 K	−0.45 K
f/k_B	−0.08 K	−0.06 K
c_v: $(k + 1.7f)/k_B$	−0.77 K	−0.55 K
χ: $(k + 2.7f)/k_B$	−0.85 K	−0.61 K

At first sight, the results for k look smaller than those reported in the literature. But keep in mind that most experiments so far were fitted by means of a TLS approach. Therefore we have also listed such 'effective' parameters as emerge from an equivalent fit within the TLS model. These values are in line with those reported by other authors. The above parameter set is also in good agreement with restrictions arising from the WKB formula (2). Then the corresponding restrictions concern both the ratio

$$\frac{f}{k} = \exp\left\{-\frac{\sqrt{2mV_0}}{2\hbar}d(\sqrt{2} - 1)\right\} \tag{19}$$

and the ratio of the isotope effect:

$$\frac{^6k}{^7k} = \exp\left\{-\frac{d\sqrt{2V_0}}{2\hbar}(\sqrt{^6m} - \sqrt{^7m})\right\}.$$

(20)

The tunnelling distance $d \approx 1.4$ Å and the mass m of lithium are known; the height of the barrier V_0 between all wells should be of the same order of magnitude. The ratios proposed above ($f/k \approx 0.13$ and $^6k/^7k \approx 1.4$) are then consistent with $V_0 \approx 200$ K and $V_0 \approx 140$ K respectively. This seems a rather reasonable value for the barrier height. So the above-given parameter set is at least consistent with the given data. We would not like to go further than this statement, but simply stress that the ESS is not in contradiction with experimental data. Furthermore, it reflects much better the microscopic picture that we have in mind when talking about a substitutional defect. Still, the TLS seems useful: it has almost the same temperature dependence of the specific heat and the static susceptibility, and is of course much simpler. Nevertheless, there appear to be some aspects which the TLS cannot reproduce at all. In the following, we will discuss these aspects.

In section 3, such properties arise from the tunnelling parameters f and r; we will show that these features make it possible to measure the tunnelling parameters directly. The properties described in section 4 are based on the particular geometric structure of the ESS; this structure leads to selection rules which cannot be understood within the framework of a one-dimensional model such as the TLS.

3. Interaction with external fields

As mentioned above, the defects exhibit both electric and elastic moments; they hence couple to the corresponding external fields. The main effect of static fields is a modification of the energy levels, whereas oscillating fields lead to characteristic transition rules. We will discuss the features in three steps. First, we look at the defect under pressure, and, second, we look at the defect under the influence of a static electric field. For both cases we look at the field dependence and the selection rules for transitions induced by acoustic and electromagnetic waves. On the basis of these results we finally propose an experiment which can determine the tunnelling parameter f (face diagonal tunnelling). Indeed, in sections 3.1 and 3.2 we will focus on situations where f becomes visible.

3.1. The defect under pressure

Let us begin by considering a defect under the influence of external pressure. As discussed before (see equation (9)), the defect exhibits an elastic quadrupole moment $Q_{ij} \propto r_i r_j (1 - \delta_{ij})$ which interacts with the strain field ε_{ij}. The latter can be derived by elastomechanical equations from the pressure exerted on the system [3]. The interaction energy (cf. section 2) reads $W_\varepsilon = -g \sum_{ij} Q_{ij} \varepsilon_{ij}$. Since Q_{ij} has (by definition) no diagonal part, the diagonal part of the strain field is irrelevant for the interaction. This fact simplifies the discussion considerably: the diagonal part of the strain field depends on the pressure in a rather non-trivial way.

The energy eigenvalue problem of a defect in an arbitrary strain field (i.e. uniaxial pressure in an arbitrary direction) is not analytically solvable. Yet some constellations with high symmetry can be solved by means of group theory. Such tractable cases appear for uniaxial pressure in the [100], [110], and [111] directions. Let us write down the interaction Hamiltonian for these cases. In order to do so, one has to derive the strain field which arises

from the exerted pressure [3]. For the cases that we consider, these strain fields and the corresponding interaction energies are listed in table 2.

Table 2. The distortion field and interaction energy for different directions.

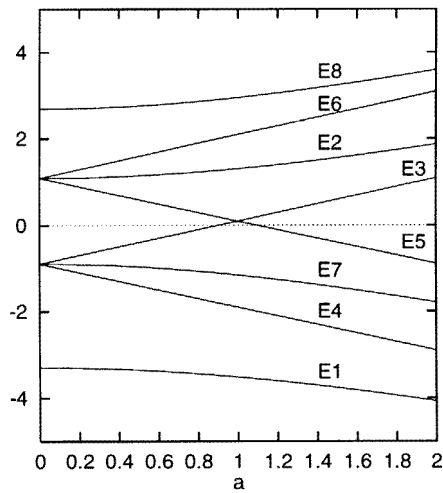| Direction of uniaxial pressure	Distortion field ε	Interaction energy W_ϵ
[001]	$\varepsilon_{ij} = \begin{pmatrix} \varepsilon_1 & 0 & 0 \\ 0 & \varepsilon_2 & 0 \\ 0 & 0 & \varepsilon_2 \end{pmatrix}$	0
[011]	$\varepsilon_{ij} = \begin{pmatrix} \varepsilon_1 & 0 & 0 \\ 0 & \varepsilon_2 & \varepsilon \\ 0 & \varepsilon & \varepsilon_2 \end{pmatrix}$	$-\dfrac{4g\varepsilon}{d^2}(1 \otimes \sigma_z \otimes \sigma_z)$
[111]	$\varepsilon_{ij} = \begin{pmatrix} \varepsilon_1 & \varepsilon & \varepsilon \\ \varepsilon & \varepsilon_1 & \varepsilon \\ \varepsilon & \varepsilon & \varepsilon_1 \end{pmatrix}$	$-\dfrac{4g\varepsilon}{d^2}(1 \otimes \sigma_z \otimes \sigma_z + \sigma_z \otimes 1 \otimes \sigma_z + \sigma_z \otimes \sigma_z \otimes 1)$

Figure 3. Energy levels of an ESS (in units of k) versus $a = 4g\varepsilon/d^2$, which is proportional to the uniaxial pressure in the [110] direction.

The off-diagonal elements ε of the strain fields are proportional to the pressure; the proportionality factor depends on the crystal's elasticity modulus. The case of exerting pressure in the [100] direction turns out to be trivial, since the strain field then has no off-diagonal elements and the interaction energy thus vanishes. The eigenvalue problems for the other two cases have been discussed in a two-level approximation (i.e. for $f = r = 0$) by Gomez *et al* [5]. We want to avoid this approximation, and focus on the case where the pressure is exerted in the [110] direction (a general discussion can be found in [12]). In this situation the Hamiltonian of a defect under uniaxial pressure reads

$$H = H_0 - \frac{4g\varepsilon}{d^2}(1 \otimes \sigma_z \otimes \sigma_z). \tag{21}$$

We will not write down any formulae concerning the eigenvalues and eigenvectors (which

can be found in reference [12]); instead we will plot all of the interesting information and give a discussion.

Figure 3 shows the dependence of the energy levels on the pressure. The energies labelled E3, E4, E5, and E6 grow linearly with pressure; the others vary quadratically for small pressure and then end up in a linear regime. All degeneracies are obviously lifted. With growing pressure, the spectrum changes from four almost equidistant levels to four doublets; the energy difference inside such a doublet is asymptotically of the order of f. The upper two doublets are separated by a gap from the lower two; this gap varies (asymptotically) linearly with pressure, whereas the distance of the doublet splitting approaches $\sim 2k$.
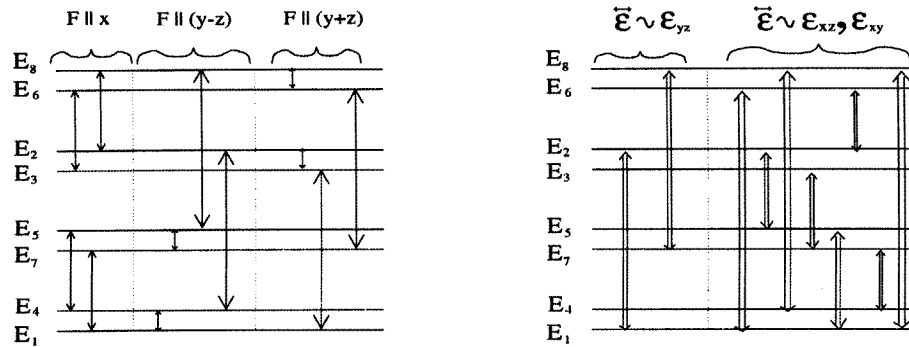

Figure 4. Energy levels of an ESS with uniaxial pressure in the [110] direction, and the electric (left-hand diagram, single arrows) and acoustic (right-hand diagram, double arrows) transitions.

Figure 4 shows the possible electromagnetic and acoustic transitions; the pressure is chosen such that the coupling energy is roughly the same as the tunnelling energy. In the left-hand part of the scheme, single arrows indicate a dipole transition (microwaves), and in the right-hand part, double arrows denote quadrupole transitions (acoustic waves). The symbol F here stands for the electric field of the electromagnetic wave, and ε for the (symmetric) distortion field of the acoustic wave (with $\epsilon_{ij} = 1$ for row index i and column index j). The scheme shows that most transitions can be induced by making an appropriate choice of the direction of the oscillating fields; in particular the frequency $\sim f$ can be induced by a microwave field with F oscillating in the [110] direction.

3.2. The defect in the presence of a static electric field

Let us now consider the defect in a static electric field (cf. equation (7)). The energy of the coupling between the field and the defect reads $W_F = -\sum_i F_i p_i$. Again, the general situation of a defect in an electric field of arbitrary direction is not analytically solvable. Two possible restrictions allow such a solution to be obtained. One of them is to neglect f and r; in this 'two-level approximation' the Hamiltonian $\hat{H} = \hat{H}_0 - F \cdot r$ factorizes into three two-dimensional problems. It is then easy to derive the spectrum and the transitions. This has been done by Gomez *et al* [5] for special symmetries, but it is in fact possible for arbitrary directions of the electric field. The second possibility is to consider cases where the electric field points along the [100], [110], and [111] directions. The resulting problem then still has a high symmetry, and group theory makes it possible to find a solution even for finite f and r. The interesting new feature emerging is the occurrence of transition

frequencies proportional to f (neglecting r) in the [110] and [111] cases. These transitions are interesting since they allow a direct measurement of f (which will be discussed below). We will consider the [111] case here; the others can be found in reference [12].
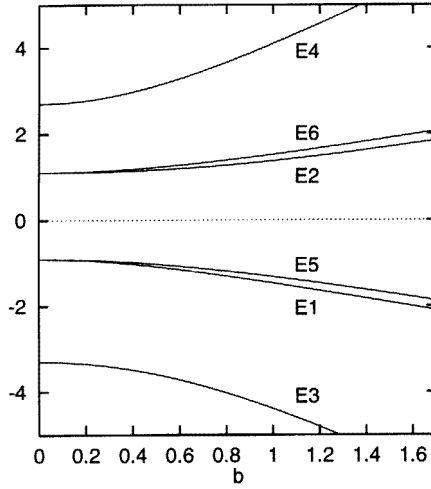

Figure 5. Energy levels of an ESS (in units of k) versus $b = pF/\sqrt{3}|k|$, which is essentially the static electric field in the [111] direction.

The Hamiltonian for a defect with an electric field in the [111] direction reads

$$H_{(111)} = k(1 \otimes 1 \otimes \sigma_x + 1 \otimes \sigma_x \otimes 1 + \sigma_x \otimes 1 \otimes 1)$$
$$+ f(1 \otimes \sigma_x \otimes \sigma_x + \sigma_x \otimes 1 \otimes \sigma_x + \sigma_x \otimes \sigma_x \otimes 1) + r(\sigma_x \otimes \sigma_x \otimes \sigma_x)$$
$$- q\frac{d}{2}F_{\text{stat}}(1 \otimes 1 \otimes \sigma_z + 1 \otimes \sigma_z \otimes 1 + \sigma_z \otimes 1 \otimes 1). \tag{22}$$

The presence of the exterior field breaks the cubic symmetry (O_H) of the defect. In the case considered, one is left with the so-called C_{3v} symmetry group (i.e. there is one threefold axis and there are three vertical reflection planes). Group theory then shows that the spectrum consists of four singlets and two doublets, since the eight-dimensional representation decomposes into four one-dimensional and two two-dimensional irreducible representations. Correspondingly, it is possible to block-diagonalize the Hamiltonian. These blocks can then be treated in (degenerate) perturbation theory, since $f, r \ll k, pF$. Again we refrain from writing down details, and instead restrict ourselves to a discussion of the results.

In figure 5 the eigenvalues are plotted against the static field F_{stat}. In contrast to the level shift due to pressure, there is no linear field dependence of any energy level. Neglecting f and r, the spectrum conserves the 1:3:3:1 degeneracy scheme. The four levels simply spread with increasing field as $2\sqrt{k^2 + (qdF/2)^2}$. Considering finite f and r changes the situation. The most remarkable new feature is the splitting of the threefold-degenerate states into a singlet (E_1, E_2) and a doublet (E_5, E_6). This splitting is proportional to the face diagonal tunnelling parameter f; it is given by

$$E_1 - E_5 = E_2 - E_6 = f \frac{3(pF/\sqrt{3})^2}{(pF/\sqrt{3})^2 + k^2}. \tag{23}$$
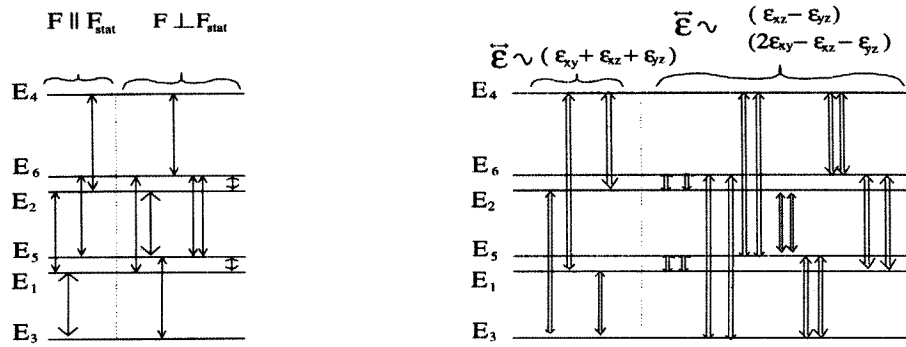
Figure 6. Energy levels of an ESS with the electric field in the [111] direction, and the electric (left-hand diagram, single arrows) and acoustic (right-hand diagram, double arrows) transitions.

Figure 6 gives the transition scheme of the situation. In the left-hand part of the scheme, we again show the dipole transitions. Two cases are listed: one where the electric field of the microwaves oscillates in line with the static field, and one where it oscillates in a perpendicular direction.

Suppressing amplitudes $\propto |f/k|^2$, we find in the first case four transitions; the selection rules remain essentially unaltered and lead to transitions of the order of $\sim 2k$. If the oscillating field is perpendicular to the static field, many transitions are possible: those 'over the gap' with a frequency growing with increasing static field, as well as those taking place 'inside' a triplet. The frequency of the latter is asymptotically determined by f. The probability for the dipole transition grows with the amplitude of the static field, $\propto F_{\text{stat}}^2$.

The acoustic selection rules are shown in the right-hand part of figure 6. There are a whole variety of possible transitions; again we want to focus on the one with frequency f. The distortion tensor ε_{ij} for such a transition has to be proportional to

$$a_1(2\epsilon_{xy} - \epsilon_{xz} - \epsilon_{yz}) + a_2(\epsilon_{xz} - \epsilon_{yz})$$

with arbitrary a_i. One possible choice is a sound wave propagating along the $(y$–$z)$ direction being polarized in the x-direction. The transition amplitude of such a constellation is given by

$$\left| \frac{k^2 - 2(qdF_{\text{stat}}/2)^2}{k^2 + 2(qdF_{\text{stat}}/2)^2} \right|^2 .$$

The increasing static field reduces the amplitude, which vanishes for $F_{\text{stat}} = \sqrt{2}kqd$. For coupling energies greater than the tunnelling energy, the transition probability then increases again.

3.3. Measuring the face diagonal tunnelling

The results of the preceding sections show that there are different possibilities for measuring the face diagonal tunnelling parameter involving choosing an appropriate geometric constellation for the exterior static and oscillating fields. Let us focus in the following on the situation of a static electric field pointing along the [111] direction (cf. section 3.2). The electric field of the microwave is assumed to oscillate perpendicularly to the static field (for example, in the $[0, 1, -1]$ direction). The selection rules tell us that a transition with frequency $\sim f$ (which should be about 100 mK) is possible. In order to have a transition rate

of the order of unity, one has to apply a static field which leads to an interaction energy of the order of k. This is fulfilled if $pF \approx k$. Since the dipole moment of the defect is known to be $p \approx 2.6D$ and $k \approx 1$ K (cf. [4]), the field strength should be $F_{\text{stat}} \approx 10^6$–$10^7$ V m^{-1}. As far as we are aware, such an experiment has never been performed.

4. Strongly coupled pairs

In section 2 we argued that a substitutional defect exhibits an electric as well as an elastic moment. These momenta lead to a coupling of the defects to external fields; moreover they produce an interaction between neighbouring defects. Here again both are present, the quadrupole coupling of the elastic moments and the dipole–dipole coupling of the electric moments. In potassium chloride doped with lithium, the electric interaction dominates the elastic coupling by an order of magnitude. Hence only the dipole–dipole interaction

$$W = \frac{1}{4\pi\varepsilon\varepsilon_0}\left(\frac{\boldsymbol{p}_1 \cdot \boldsymbol{p}_2}{R^3} - 3\frac{(\boldsymbol{p}_1 \cdot \boldsymbol{R})(\boldsymbol{p}_2 \cdot \boldsymbol{R})}{R^5}\right) = \frac{J}{4}(\boldsymbol{e}_1 \cdot \boldsymbol{e}_2 - 3(\boldsymbol{e}_1 \cdot \boldsymbol{e}_R)(\boldsymbol{e}_2 \cdot \boldsymbol{e}_R)) \tag{24}$$

with

$$J = \frac{1}{\pi\varepsilon\varepsilon_0 R^3}\frac{p^2}{3} \tag{25}$$

is relevant. Here $\boldsymbol{p}_i$ denotes the dipole moment of defect i, $\boldsymbol{R}$ is the vector connecting the defects, the $\boldsymbol{e}$s are $\boldsymbol{e} = (2/d)\boldsymbol{r}$, and ε_0 and ε are the dielectric constant of the vacuum and of the potassium chloride matrix respectively.

The structure of the host crystal confines the defects to discrete sites on the lattice. Hence the possible distances between the pairs will be a discrete set. Although this fact is irrelevant for the bulk of the pairs which have a distance of, say, ten lattice constants or more (the crystal then appears as a quasicontinuum), it is most relevant for the strongly coupled pairs which we will consider here. Geometric considerations show that, on the fcc lattice, the nearest neighbours NN1 lie along the $[1/2, 1/2, 0]$ directions and the next-nearest neighbours NN2 lie along the $[1, 0, 0]$ direction. Comparing the energy scales for neighbouring pairs, one finds that the interaction energy dominates the ESS tunnelling parameters. This can be estimated by evaluating the dipole–dipole interaction (24) using the lattice constant $a \approx 6.23$ Å and the dipole moment $p \approx 2.6D$. For the nearest neighbours NN1 one is led to a value of $\varepsilon J \approx 710$ K (evaluated with $R = a/\sqrt{2}$). In order to determine the value of the coupling, one has to specify the dielectric constant of the material. Yet on the atomic length scale it is not clear which value to take for this constant; at least one can confine it to the interval $\varepsilon(\text{vacuum}) = 1 < \varepsilon < \varepsilon(\text{KCl}) = 4.25$. This tolerance leads to values 170 K $< J_{\text{NN1}}/k_B <$ 710 K. For the next-nearest neighbours NN2 the interval is 60 K $< J_{\text{NN2}}/k_B <$ 250 K. This estimation, rough as it is, shows that the coupling between neighbouring defects exceeds by at least one order of magnitude the intrinsic energy scales (which are given by $k \approx 1$ K). The strongly coupled pairs hence constitute a composite degree of freedom which should be considered as a unit.

Klein [11] and one of the authors [10] have discussed defect pairs in the two-level approximation; within this approximation one can predict the existence of a small frequency $4k^2/J$ for strongly coupled pairs. For nearest or next-nearest neighbours this energy should be between 5 mK and 50 mK. Weis *et al* [9] investigated the system experimentally by measuring Rabi frequencies in spin-echo experiments. They found a broad distribution of frequencies in the 10 mK region; in addition there was a rather narrow distribution of Rabi

frequencies:

$$\Omega_R \propto \frac{4k^2/J}{E} \boldsymbol{F} \cdot \boldsymbol{p}.$$

The analysis of these experiments was first done by considering the strongly coupled pair as an effective TLS with a tunnelling rate $4k^2/J$ and an asymmetry Δ. The total energy of such an effective TLS then reads $E = \sqrt{\Delta^2 + (4k^2/J)^2}$ (which is the resonance energy of the external field). Weis now argued that the measured frequency distribution is due to a distribution of the asymmetry Δ. Such a distribution arises from imperfections of the probe, whereas there is no plausible reason for a distribution of the dipole moment.

Still, the existence of only one frequency was somewhat striking; obviously only one pair constellation contributed to the signal (otherwise additional Rabi frequency peaks would appear). In order to explain this puzzle, Würger [4] discussed a pair of ESS using perturbation theory. He showed that only the pair constellation NN2 has a frequency in the range between 5 mK and 50 mK. For all other constellations, geometric selection rules prohibit transitions with these energies. He also showed that an asymmetry proportional to the position operator explains the distribution of frequencies. Yet he left open the question of which role other forms of asymmetries (e.g. a 'quadrupole asymmetry' proportional to $r_i r_j$ which couples to internal strain fields) will play.

In order to treat this problem, one can discuss the NN1 and NN2 cases applying group theory and tensor factorization. In this context, all types of asymmetry are easily discussed, considering them as small perturbations. We restrict ourselves to a brief overview of the proposed methods, and present the results for the NN2 constellation (for details, cf. [12]).

First, the basis $\{|xyz\rangle\}$ for one defect is expanded to $\{|x_1 x_2 y_1 y_2 z_1 z_2\rangle\}$ for the pair. In this basis the Hamiltonian reads

$$H = H_0 + W \tag{26}$$

where H_0 stands for the tunnelling energy of both defects, and W denotes the dipole interaction. This (64-dimensional) Hamiltonian does indeed factorize, just as in the case of a single defect (we write k_i for the edge tunnelling rate of the defect i):

$$
\begin{aligned}
H = {} & \left(k_1(\sigma_x \otimes 1) + k_2(1 \otimes \sigma_x) - \frac{J}{2}(\sigma_z \otimes \sigma_z)\right) \otimes \mathbf{1}_{4\otimes 4} \otimes \mathbf{1}_{4\otimes 4} \\
& + \mathbf{1}_{4\otimes 4} \otimes \left(k_1(\sigma_x \otimes 1) + k_2(1 \otimes \sigma_x) + \frac{J}{4}(\sigma_z \otimes \sigma_z)\right) \otimes \mathbf{1}_{4\otimes 4} \\
& + \mathbf{1}_{4\otimes 4} \otimes \mathbf{1}_{4\otimes 4} \otimes \left(k_1(\sigma_x \otimes 1) + k_2(1 \otimes \sigma_x) + \frac{J}{4}(\sigma_z \otimes \sigma_z)\right).
\end{aligned}
\tag{27}
$$

We are left with three four-dimensional problems. After this factorization it is easy to derive the complete spectrum together with all of the selection rules. This spectrum consists of different multiplets, which are separated by gaps of the order of $\sim J/4$. For the experiments considered, the temperature is much lower than this energy, and hence only the lowest level group is of interest. In the middle of figure 7 the spectrum of this lowest multiplet is shown together with the dipole selection rules. It consists of eight states with a degeneracy scheme 1:1:2:2:1:1. The energy eigenvalues are typically each the sum of three roots of the form $\sqrt{(J/4)^2 + (k_1 \pm k_2)^2}$ and $\sqrt{(J/2)^2 + (k_1 \pm k_2)^2}$.

In order to determine the transitions caused by an external field, one has to consider an interaction with the two defects: $W_F = -\boldsymbol{F} \cdot (\boldsymbol{p}_1 + \boldsymbol{p}_2)$. The spatial dependence of F is neglected, since the wavelength of F (≈ 1 cm) is much greater than the distance of the two defects (≈ 10 Å). There is only one transition frequency (just as in the case of a single

defect). But here transitions are only induced by electric fields $\boldsymbol{F}$ oscillating in line with the distance vector $\boldsymbol{R}$.

The structure of the spectrum together with the selection rules makes it again possible to talk about the pair as an effective TLS with tunnelling rate $4k_1k_2/J$. In particular, it is possible to use the well-known Rabi formalism for the TLS in order to interpret the echo experiments. In a way this is an *a posteriori* justification of the TLS approximation which had been proposed in the context of defect pairs [10].

Considering an asymmetry is now somewhat more complicated than in the two-level approximation. There the asymmetry was simply proportional to the one-dimensional position operator. The ESS is in a sense three dimensional, and one has to find a way to assign a different potential value to each well. This can be done by introducing three dipole terms, three quadrupole terms, and an octupole term. Allowing different asymmetries at the two defects, one gets

$$V_d = \sum_{i=x,y,z} v_i(r_i^1 + r_i^2) + \delta v_i(r_i^1 - r_i^2) \tag{28}$$

$$V_q = \sum_{\substack{i,j=x,y,z \\ i \neq j}} v_{ij}(r_i^1 r_j^1 + r_i^2 r_j^2) + \delta v_{ij}(r_i^1 r_j^1 - r_i^2 r_j^2) \tag{29}$$

$$V_o = v_{xyz}(r_x^1 r_y^1 r_z^1 + r_x^2 r_y^2 r_z^2) + \delta v_{xyz}(r_x^1 r_y^1 r_z^1 - r_x^2 r_y^2 r_z^2) \tag{30}$$

with the mean asymmetry $v = (v_1 + v_2)/2$, and the difference $\delta v = (v_1 - v_2)/2$. The existence of dipole and quadrupole asymmetries is plausible since it can be deduced from electric and elastic internal fields which couple weakly to an arbitrarily chosen defect. In contrast, the octupole term has no such explanation, and we hence neglect it in the following. The asymmetries V_d and V_q will be of the same order of magnitude as $4k_1k_2/J$. Treating them properly, one is led to the following conclusions.

(i) We find that the part of the dipole mean asymmetry which is parallel to the distance vector $\boldsymbol{R}$ alters the frequency to $\sqrt{(4k_1k_2/J)^2 + v^2}$; this result is consistent with that proposed by Würger [4].

(ii) None of the other terms (such as the quadrupole terms) change the transition frequency; neither does the difference in asymmetry.

These results are shown in figure 7. In the middle we show the lowest multiplet without asymmetry; on the right-hand side we show the 'dipole asymmetry' changing the energy levels, and on the left-hand side we show the 'quadrupole asymmetry', simply shifting the levels without changing the frequencies of the allowed transitions. The experiments performed by Weis are hence only sensitive to the *mean dipole asymmetry*. No other forms of asymmetry play a significant role here.

5. Conclusion

In this article we had the aim of comparing the physics of a two-level system (TLS) to that of an eight-state system (ESS). Both systems are used as possible models for cubic substitutional defects such as the lithium atom in a KCl host lattice. The ESS reflects much better our microscopic picture of the defect, and it is hence interesting to know what features are left out of consideration when treating the defect as a TLS.

Using a tensorial notation, we reminded the reader that the ESS reduces to three TLS if tunnelling along the face and space diagonal of the cube is neglected. Then we presented three contexts in which differences between the two models arise.
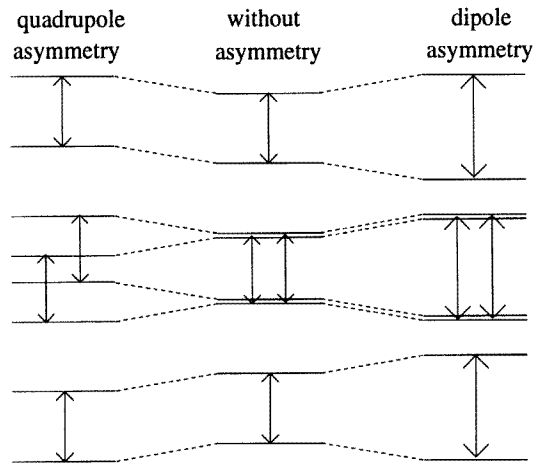
Figure 7. The lowest multiplet of NN2.

First, we looked at the temperature dependence of the specific heat and of the static dielectric susceptibility. A simple way to summarize the differences of the models is to state that for the TLS the relation $k^2 \partial_T \chi = c_v$ holds, whereas this is not true for the ESS. In particular, the maximum temperature of the specific heat and the turning point of the susceptibility coincide for the TLS, whereas they are different for the ESS. We think that the experimental data do indeed show this tendency. The ratio f/k (face to edge tunnelling) and the isotope effect $^6k/^7k$ estimated from the data lead to reasonable orders of magnitude for the barrier height (100–200 K).

Second, we investigated the differences of the two models in the presence of external forces (uniaxial pressure and a static electric field). There appear different aspects where tunnelling along the face and space diagonal of the cube is visible. These features make it possible to set up a resonance experiment where the face diagonal tunnelling can be measured directly: applying the electric field along the [111] direction, there are (both acoustic and electromagnetic) transitions with frequencies $\omega \sim f(pF)^2/((pF)^2 + k^2)$ (where p denotes the dipole moment and F the static electric field). Of course such features cannot be described within the framework of a TLS.

As a third context, we discussed strongly coupled defect pairs. Here again some properties arise that cannot be explained by a two-level approximation. For strongly coupled pairs, *geometric* selection rules inhibit transitions for some constellations (such as the nearest neighbours). In addition, different asymmetry terms are possible for an ESS, whereas in the TLS only one such term appears. It is because of the interplay of the selection rules and the structure of the spectrum that these other asymmetries are not observable in the echo experiments performed. This is why the situation can be described in terms of an effective TLS.

We thus conclude that there are a number of situations in which the ESS shows observable features which cannot be described by a TLS. Nevertheless, the latter is a good approximation in all contexts where the geometry and the parameters for tunnelling along the face and space diagonal are of no relevance. In these situations, the TLS, being the simplest model for a tunnelling degree of freedom, does in fact sketch all of the essential features of the defect.

Acknowledgments

References

[1] Narayanamurti V and Pohl R O 1970 *Rev. Mod. Phys.* **42** 201
[2] Harrison J P, Peressini P P and Pohl R O 1968 *Phys. Rev.* B **171** 1037
[3] Landau L D and Lifshitz E M 1983 *Elastizitätstheorie (Lehrbuch der Theoretischen Physik VII)* (Berlin: Akademie)
[4] Würger A 1996 *From Coherent Tunneling to Relaxation (Springer Tracts in Modern Physics 135)* (Heidelberg: Springer)
[5] Gomez M, Bowen S P and Krumhansl J A 1967 *Phys. Rev.* B **153** 1009
[6] Enss C, Gaukler M, Hunklinger S, Tornow M, Weis R and Würger A 1995 *Phys. Rev.* B at press
[7] Kubo R, Toda M and Hashistume N 1985 *Statistical Physics* (Heidelberg: Springer)
[8] Fiory A T 1971 *Phys. Rev.* B **4** 614
[9] Weis R, Enss C, Würger A and Lüty F 1996 Coherent tunneling of lithium defect pairs in KCl crystals *Preprint*
[10] Terzidis O and Würger A 1996 *J. Phys.: Condens. Matter* **8** 7303
     Terzidis O and Würger A 1994 *Z. Phys.* B **94** 341
[11] Klein M W and Wang Z H 1986 *Phys. Rev. Lett.* **57** 1355
     Klein M W 1984 *Phys. Rev.* B **29** 5825
[12] Nalbach P 1996 *Diploma Thesis* Ruprecht-Karls-Universität Heidelberg